DMD Fast Forward. Published on February 20, 2019 as DOI: 10.1124/dmd.118.085787
This article has not been copyedited and formatted. The final version may differ from this version.

The Time-course of Aldehyde Oxidase and the Reason Why it is Nonlinear

Armina Abbasi, Erickson M. Paragas, Carolyn A. Joswig-Jones,

John T. Rodgers, and Jeffrey P. Jones

Department of Chemistry, Washington State University, Pullman, WA 99164-4630

Running title: Why is AO nonlinear over time?

Corresponding author:
Jeffrey P. Jones, Ph.D.
Department of Chemistry
Washington State University
Pullman, WA 99164-4630
Tel: +1(509) 592-8790
E-mail: jpj@wsu.edu

Number of pages: 40

Number of Figures: 8

Number of Tables: 3

Number of references: 40

Number of words in Abstract: 225

Number of words in Introduction: 624

Number of words in Discussion: 1251

Abbreviations: [2Fe-2S], iron-sulfur cluster; 5NQ, 5-nitroquinoline; AIC, Akaike information criterion; AOX, aldehyde oxidase; CL_{int}, intrinsic clearance; DACA, N-(2-dimethylamino)ethyl)acridine-4-carboxamide; DMSO, dimethyl sulfoxide; EDTA, ethylenediaminetetraacetic acid; FAD, Flavin adenine dinucleotide; HAO, purified expressed human aldehyde oxidase; HLC, human liver cytosol; K_m, Michaelis-Menten constant; K_I, dissociation constant for substrate inhibition; Ki, equilibrium dissociation constant for a

competitive inhibitor; MA, multispecies allometry; MAM, modulated activity model; MM, Michaelis-Menten; MoCo, molybdenum pterin cofactor; O6BG, O^6-benzylguanine**;** PAR, peak area ratio**;** ROS, reactive oxygen species; SOD, superoxide dismutase; SSS, single-species scaling; TDI, time dependent inhibitor; LC-MS/MS, liquid chromatography-tandem mass spectrometry; V_{MAX}, maximum velocity; V/K, intrinsic clearance.

Abstract:

Many promising drug candidates metabolized by Aldehyde Oxidase (AOX) fail during the clinical trial due to underestimation of their clearance. AOX is species specific and this makes traditional allometric studies a poor choice for estimating human clearance. Other studies have suggested using half-life calculated by measuring substrate depletion to measure the clearance. In this study, we are proposing using numerical fitting to enzymatic pathways other than Michaelis-Menten (MM) to avoid missing the initial high turn-over rate of product formation. Here, product formation over 240-minute time-course of six AOX substrates, O^6-benzylguanine, DACA, zaleplon, phthalazine, BIBX1382 and zoniporide have been provided to illustrate enzyme deactivation over time to help better understand why MM kinetics sometimes lead to underestimation of rate constants. Based on the data provided in this paper, the total velocity for substrates becomes slower than the initial velocity by 3.1, 6.5, 2.9, 32.2, 2.7 and 0.2 fold respectively in human expressed purified enzyme (HAO) while the K_m remains constant. Also, our studies on the role of reactive oxygen species (ROS) such as superoxide and hydrogen peroxide shows that ROS did not significantly alter the change in enzyme activity over time. Providing a new electron acceptor, 5-nitroquinoline, did however alter the change in rate over time for a number of compounds. The data also illustrate the difficulties in using substrate disappearance to estimate intrinsic clearance (V/K).

DMD Fast Forward. Published on February 20, 2019 as DOI: 10.1124/dmd.118.085787
This article has not been copyedited and formatted. The final version may differ from this version.

Introduction:

Aldehyde oxidase (AOX) is a cytosolic protein belonging to the family of molybdoflavoenzymes (Mendel, 2009). It is found most extensively in liver but it is also expressed in kidney, lungs, the gastrointestinal tract and skin. AOX is a homodimer enzyme that needs four cofactors in each one of its 150 kDa subunits to be active. These cofactors including molybdenum pterin cofactor (MoCo), two iron-sulfur clusters [2Fe-2S] and a flavin adenine dinucleotide (FAD) site (Garattini et al., 2008; Mendel, 2009). The final electron acceptor for the flow of electrons from the MoCo site to the flavin site is molecular oxygen which forms reactive oxygen species (ROS) $O_2^{\bullet-}$ and H_2O_2. AOX is capable of both oxidative and reductive transformations of a wide range of compounds. AOX oxidative substrates include aldehydes, aromatic heterocycles, iminium ions and azaheterocycles. While AOX reductive substrates include sulfoxides, nitro compounds, *N*-oxides, nitrates, nitrites and molecular oxygen (Krenitsky et al., 1972; Kitamura and Tatsumi, 1984; Stoddart and Levine, 1992; Li et al., 2009b; Pryde et al., 2010; Maia et al., 2015). AOX reductions have recently been gaining attention (Konishi et al., 2017; Paragas et al., 2017a; Amano et al., 2018). Previously, it was believed that AOX reduction only occurs under anaerobic conditions (Li et al., 2009a; Weidert et al., 2014; Maia et al., 2015). recently it was proved that reduction by AOX can also occur under normal oxygen condition and at a different site than where substrate oxidation happens.

More than 90% of metabolic breakdown of drugs and xenobiotics is through the P450 family of enzymes (Lynch and Price, 2007). However, recent efforts toward making drugs more stable to P450 metabolism has also had the effect of making them susceptible to clearance by other pathways. This has turned the attention to studying other enzymatic pathways, particularly AOX,

in drug metabolism. Although extensive studies have been done on prediction of intrinsic clearance (CL_{int}) for P450-cleared compounds (Dalvie et al., 2010a), the ability to obtain a close estimation of in vivo clearance from in vitro data for AOX-mediated metabolism has not yet been developed. Traditional allometric scaling assumes that drug elimination mechanism is conserved across species but this is not the case for AOX since there is a noticeable difference in AOX activity between human and preclinical species. In species, such as rat and mouse, substrate is metabolized by different isoenzymes, AOX1 and AOX3, while it is not metabolized at all by AOX in dogs, which do not produce active AO (Kaye et al., 1984; Dalvie et al., 2010b; Garattini and Terao, 2012). Recent efforts to predict clearance have used novel allometric studies using single-species scaling (SSS) or multispecies allometry (MA) to scale in vitro CL_{int}, rat, guinea pig, monkey and minipig to human in vitro CL_{int} (Crouch et al., 2018). Another method proposed to predict in vivo metabolism from in vitro CL_{int} is by monitoring substrate depletion in time and then use the half-life to scale up the results to the whole human body (Zientek et al., 2010).

Atypical kinetics of cytochrome P450 family of enzymes has already been extensively studied (Korzekwa et al., 1998; Hutzler and Tracy, 2002). However, this kind of behavior is not specific to that family. Many AO substrates deviate from Michaelis-Menten (MM) steady state kinetics. The enzyme is nonlinear over time and it is apparent that multiple substrate can bind to the enzyme resulting in substrate inhibition (Barr et al., 2014). MM kinetics requires a single active site per enzyme and it also requires each site to operate independently from others in a homodimeric protein.

In this paper, we have used three enzyme systems, human liver S9 fraction, human liver cytosol (HLC) and purified expressed human AOX (HAO) to monitor product formation over a 240-minute time course for six substrates. We evaluate whether product is formed at a constant rate over the time course, which we define as a linear time course, or if the enzyme changes rate over time (nonlinear). Furthermore, since oxygen plays an important role in the enzyme cycle as the ultimate electron acceptor (Pryde et al., 2010), we check for any loss of activity related to oxygen consumption or reduction during the catalytic cycle by using superoxide dismutase (SOD) and catalase to remove ROS and determine the affinity of oxygen for human AO.

DMD Fast Forward. Published on February 20, 2019 as DOI: 10.1124/dmd.118.085787
This article has not been copyedited and formatted. The final version may differ from this version.

Materials and methods:

N-(2-dimethylamino)ethyl)acridine-4-carboxamide (DACA) was synthesized as described previously (Paragas et al., 2017b). O^6-benzylguanine (O6BG) and zaleplon, were purchased from Toronto Research Chemicals (ON, Canada), zoniporide and dantrolene from Cayman Chemical Company (Ann Arbor, MI), BIBX1382 from Tocris Bioscience (Bristol, UK), and internal standards (phenacetin and 2-methly-4(3*H*)-quinazolinone), phthalazine, protocatechuic acid, protocatechuate 3,4-dioxygenase (*Pseudomonas sp*.), glucose oxidase (*Aspergillus sp.*), glucose, catalase (bovine liver), and superoxide dismutase (SOD, bovine erythrocytes) were purchased from Sigma-Aldrich (St. Louis, MO). The standard metabolites were synthesized and purified as previously described (Paragas et al., 2017b) except 1-phthalazinone which was purchased from Sigma-Aldrich (St. Louis, MO). 5-nitroquinoline was purchased from TCI America (Portland, OR). The monobasic potassium phosphate, dibasic potassium phosphate and ethylenediaminetetraacetic acid (EDTA) used for the potassium phosphate buffer were purchased from JT Baker (Center Valley, PA). Human liver S9 fraction, pooled from 20 donors (gender ratio not specified, lot # 3212595), was purchaced from BD Gentest (Corning, NY). Human liver cytosol (HLC), pooled from 50 individual donors **(**30 male and 20 female, lot # 1410012**),** was purchased from XenoTech (Lenexa, KS). Expression and purification of human AOX (HAO) was performed following the method previously described (Alfaro et al., 2009; Paragas et al., 2017b). The total amount of AOX in HLC and HAO was quantified by liquid chromatography-tandem mass spectrometry (LC-MS/MS) (Barr et al., 2013).

General incubation conditions. Each incubation vial contained 5 times the K_m amount of each substrate in 25 mM potassium phosphate buffer (pH 7.4) containing 0.1 mM EDTA. Samples were

pre-incubated for 5 minutes at 37°C. The reaction was started by adding the HLC (0.0051 μM final AO concentration) or HAO (0.0192-0.043 μM). Total reaction volume was 3 ml and 200 μL of the reaction vial was taken out and quenched immediately at times 0, 2, 4, 10, 20, 30, 45, 60, 120, 240 minutes. The time points for phthalazine were slightly different, 0, 0.5, 1, 1.5, 2, 2.5, 3, 4, 5, 10, 20, 45, 75, 135, 240 minutes, due to its immediate transition to nonlinearity. Samples were quenched using 50 μL of 1 M formic acid containing known concentration of IS (either phenacetin or 2-methly-4(3*H*)-quinazolinone). Incubation with the human liver S9 fraction (20 mg/ml) was only done for the substrate O6BG as an example to check the results in a more intact cellular fraction. The samples were then centrifuged at 16,100*g* for 10 minutes in an Eppendorf centrifuge 5415D and the supernatant was collected for LC-MS/MS. For experiments done to check the effect of ROS, the incubation conditions were similar except 250 U/mL catalase and 250 U/mL of SOD were added to the reaction before pre-incubation. Same for reactions in which 5NQ was used. Five times the K_m amount of 5NQ (200 μM) in the presence of oxygen was added to the reaction before the pre-incubation. All the experiments were done in triplicates and the goodness of fits were assessed using the Akaike Information Criteria (AIC) values.

Oxygen K_m calculation. The K_m for oxygen was measured using saturating concentration of phathalazine. HLC was incubated with protocatechuate 3,4-dioxygenase (1 U/mL) and protocathechuic acid (20 mM). The oxygen concentration was monitored using Robust oxygen probe (Pyroscience, Germany). Aliquots were collected when the needed oxygen concentration was reached and added to a vial containing 50 mM phthalazine. The phthalazine assay was incubated at 37°C for 2.5 minutes. The final reaction volume was 100 μL. The reaction was

quenched by the addition of 25 μL of 1 M formic acid containing 25 μM phenacetin, as internal standard.

Data analysis. Numerical fitting in Mathematica 11.0.1.0 (Wolfram Research, Champaign, IL) was performed using the NDSolve function with MaxSteps → 10000 and PrecisionGoal → ∞ . k_1 was fixed to 270 μM s^{-1} and k_2 was set to $k_1 \times K_m$ for each substrate. Model fitting was done using the NonlinearModelFit function with 1/Y weighting. Goodness of fit was evaluated by AIC and RSquared commands. Dataset simulation was done using the rate constants derived from the numerical fitting. GraphPad Prism 7.0c (GraphPad Software Inc., San Diego, CA) was used for developing saturation curves. The data was fitted to three different kinetic models; namely, Michaelis-Menten (MM), dead model and the modulated activity model (MAM) (Fig. 4) the graphical results of the fits are given for all substrates in supplemental information (supplemental Fig. 1). Several substrate inhibition models were also developed (Supplemental Fig. 2). These models were tested on two of our substrates which were reported to exhibit substrate inhibition, DACA and phthalazine, (Obach et al., 2004; Paragas et al., 2017b). The fits to these models were either almost identical to the MAM or could not fit the data points well (Supplemental Fig. 3 and Supplemental Table 1).

Liquid Chromatography – Mass Spectrometry. Samples were analyzed using an LC-20AD series high performance liquid chromatography system (Shimadzu, Columbia, MD) fitted with an HTC PAL autosampler (LEAP Technologies, Carrboro, NC). Chromatography was performed using two columns, a Luna C18 column (50 × 2.0 mm, 5 μm; Phenomenex, Torrance, CA) and a Luna C18 column (100 × 2.0 mm, 5 μm; Phenomenex, Torrance, CA). Mobile phase A consisted of 0.05% (by volume) formic acid and 0.2% acetic acid (MilliporeSigma, Billerica, MA) in water,

and mobile phase B comprised 90% acetonitrile (MilliporeSigma, Billerica, MA), 9.9% water, and 0.1% formic acid (Fischer Scientific, Pittsburgh, PA). The quantitation was conducted on an API 4000 Q-Trap mass spectrometry system (Applied Biosystems/MDS Sciex, Foster City, CA) with turbospray ESI operating in positive ion mode. For O^6BG and 8-oxo-O^6BG, the initial condition was 10% mobile phase B and 90% mobile phase A for 0.3 minutes. The concentration of mobile phase B was ramped up to 95% at 2.2 minutes and held constant for 0.1 minutes, followed by a linear gradient back to 10% B for 0.9 min. For DACA, zaleplon, zoniporide and BIBX1382 together with their respective metabolites, the initial condition was 10% mobile phase B and 90% mobile phase A until 0.3 minutes. The concentration of mobile phase B was ramped up to 75% at 2.2 minutes and held constant for 0.1 minutes before ramping down to 10% again at 3.1 minutes and held constant for 0.9 minutes. For zaleplon the initial condition until 0.3 minutes was 10% mobile phase B and 90% mobile phase A. The concentration of mobile phase B then ramps up to 95% at 2.2 minutes and held constant for 0.1 minutes before ramping down to 10% again at 3.1 minutes and held constant for 0.9 minutes. For phthalazine the initial condition until 2 minutes was 10% mobile phase B and 90% mobile phase A. The concentration of mobile phase B then ramps up to 80% at 8 minutes and held constant for 0.5 minutes before ramping down to 10% again at 9 minutes and held constant for 1 minute. The mass spectrometer tuning parameters used for all the compounds were as follows: collision gas, medium; curtain gas, 20; ion spray voltage 4900; ion source gas 1, 35; ion source gas 2, 55; desolvation temperature 600; declustering potential, 70; entrance potential, 10; cell exit potential, 15; and the collision energy was 25 for O^6BG, DACA, zaleplon and zoniporide. The only differing factor for BIBX and Phthalazine was the collision energy which were 65 and 35 respectively. The flow rate for O^6BG, DACA, zoniporide and BIBX (including their respective metabolites) was 0.4 mL/min. The flowrate for

zaleplon and phthalazine together with their corresponding metabolites was 0.3 mL/min and 0.35 mL/min, respectively. The substrates and metabolites were detected using multiple reaction monitoring mode by monitoring the following m/z transitions: 2-oxo-zoniporide, 337 → 278 (Dalvie et al., 2010b); DACA-acridone, 310.2 → 265.0 (Barr and Jones, 2013); 8-oxo-O^6BG, 258.2 → 91 (Barr et al., 2015); 5-oxo-zaleplon, 322.3 → 280.1 (Hutzler et al., 2012); BIBU1476, 404.1 → 373.1; 3-oxo-XK469, 361.2 → 315; 1-phthalazinone, 147.1 → 118; aminodantrolene, 285.15 → 186.0 (Amano et al., 2018); and the internal standards (IS) were either 2-methyl-4(*3H*)-quinazolinone 161.0 → 120.0 or phenacetin 180.2 → 110.1, as specified. All the metabolic reactions are summarized in (Fig. 1).

Results:

Time course

The data indicates that AOX catalysis rates are not constant over time and in most cases the enzyme appears to be less active as time progresses depending on the substrate. For example, in the case of phthalazine the linear range of enzymatic activity is very short (less than 3 minutes) and in other instances such as zoniporide the enzymatic activity remains almost linear and may even increase slightly over 240-min incubation time (Fig. 2**).** It should be noted that we do not have metabolic standards for BIBX1382 and zoniporide so the rate constants are not accurate. These compounds are included since they support that most reactions are nonlinear over time. For these compounds we report peak area ratio (PAR) instead of μmoles/min.

A source of purified enzyme was used to confirm that the data from HLC is mainly the result of AOX activity and no other enzyme sources in liver cytosol. From comparing the plots for both enzyme sources, it is evident that the linearity of both sets are very similar and this suggests that the nonlinearity in time is the result of change in the activity of AOX (Fig. 3). The results from incubation of O6BG with S9 fraction shows that the same mechanism persists even in a more intact cell system (Supplemental Fig. 4).

Data fitting using Mathematica

The assumption for MM kinetics is that the enzyme produces product in a linear fashion over time. This is obviously not the case, and we could not get a good fit for this model to our results. For the dead model the differential equations are solved based on the kinetic scheme that suggests an irreversible loss of enzymatic activity over time. Finally, we tested a model in which it is assumed

that the enzyme is altered over time to have a slower rate of reaction and therefore runs with a lower efficiency after a certain period of time. This last model could be a result of a number of changes in the enzyme, such as a slow conformational change, or chemical modification, such as oxidation of amino acids by ROS.

Although in many cases the MM model gives a visually acceptable fit, the AIC values predict that the MAM, in which the enzyme activity is altered over time, is the kinetic model that describes the enzymatic behavior best with zoniporide being the only exception. The importance of using the right model can be further emphasized by seeing up to almost 40-fold difference between the rate constants related to each model in HAO or HLC (Tables 1 and 2). The differences between these rate constants are substrate specific, thus scaling is not an option and one must use the correct model to get a correct intrinsic clearance. Based on the assumption that the fast initial rate (k_3) is what happens in the in vivo situation, we can use the intrinsic clearance (V/K) and then use equation 1 to scale up the calculations to clearance per body weight. In addition, we have also done the calculations with k_5 instead of k_3 to present how missing the fast initial rate due to experimental errors in choosing the linear portion of the time-course plot may lead to underestimation of clearance by using the apparent k_3 which will be similar to k_5.

$$Cl'_{int,AO} = \frac{k3}{K_m} \times \frac{30 \times 10^{-3}\ \mu mol\ AO}{g\ liver} \times \frac{21\ g\ liver}{kg\ b.wt.} \quad (eq.1)$$

The amount of AOX in the liver in the formula above was previously calculated in our lab to be 21-40 pmol AOX/mg liver and we have used the average amount for our calculations (Barr et al., 2013). We have provided the intrinsic clearance in HAO for MAM in comparison to the linear

model and the in vivo data (Table 3). The data shows a significant improvement of in vitro clearance for the MAM. This difference becomes increasingly noticeable with longer incubation times. Unfortunately, the number of the substrates that we were able to calculate the intrinsic clearance for are few. However, the MAM data shows a great improvement for all three substrates in comparison with what was previously reported in the literature (Zientek et al., 2010)

Some potential reasons behind nonlinearity in enzyme activity

A number of mechanisms could be responsible for this loss of activity. First, we hypothesized that the loss of activity was a result of the enzyme inactivation by the reactive oxygen species (ROS) super oxide and hydrogen peroxide which is generated during the catalytic cycle. To test this theory, we used superoxide dismutase and catalase. Catalase was used to remove hydrogen peroxide and superoxide is removed by SOD. By using these two enzyme sources we expected to see an increase in the linearity of enzyme activity. No significant change in enzyme linearity was observed in either HLC or HAO. However, some inconsistencies were observed between HLC and HAO activities with or without using SOD and catalase. In the case of HLC all substrates showed some to very little improvement in activity except O6BG but in the case of HAO almost the opposite trend was observed. Unlike what happened in HLC, the activity decreased with adding oxygen species scavengers for DACA and zoniporide while it increased for O6BG. In the case of zaleplon and BIBX there was little to no improvement in activity the same as what was observed in HLC (Fig. 5 and Fig. 6). What was consistent was that in any case no improvement in linearity of the time-course plots was observed. Given these results it is not likely that ROS are not the main reason for nonlinear kinetics, although the ROS could modify the enzyme prior to diffusing away from the flavin binding site.

Substrate depletion over time

Another potential reason for the nonlinearity is a substantial decrease in the oxidative substrate concentration. The amount of substrate disappearance as calculated by the amount of product formed indicates that the amount of substrate consumed was less than 10% of the total substrate in most cases. We have simulated substrate disappearance to demonstrate this (Fig. 7) assuming 1M of product is formed from 1M of substrate. This should be the same even for the substrates that we don't have the standards for since we have used five times the K_m amount for all the substrates. This indicates that substrate depletion is not significant for the oxidative substrates. However, the reductive substrate oxygen could also be significantly depleted. In our laboratory, and under the conditions of our reaction, the oxygen concentration is very close to 213 μM. Since one to two oxygen molecules are consumed per catalytic cycle it appears that only a small fraction of the substrate oxygen is consumed. However, one might still see nonlinearity over time if the K_m value for oxygen is very high. We measured the K_m value to be around 2 μM for human AOX. To double-check our results, we have used the data published earlier for a reductive substrate of AOX, dantrolene (Amano et al., 2018). Since dantrolene gets reduced by AOX to aminodentrolene by a three step process similar to 5NQ (Paragas et al., 2017a) , it will compete for the reduction site of the enzyme with oxygen. We have used the K_{mapp} reported in the paper mentioned above for dantrolene (65 μM) and the K_m of this substrate was also measured in our lab under anaerobic condition (4.7 μM, unpublished data, manuscript in preparation). This enabled us to calculate the K_i for oxygen to be approximately 15.6 μM by using the equation $K_{mapp} = K_m (1 + [I]/K_i)$ assuming that the oxygen concentration, [I], is close to 213 μM when the atmospheric pressure ranges from 765-780 mm Hg at 37°C (Weiss, 1970). Since either way, the oxygen K_m is much smaller than its

concentration present during the reaction, depletion of the substrate oxygen is not a factor in the nonlinearity.

Using 5NQ as a reductive substrate

A third hypothesis is that maybe the enzyme is slow to reduce oxygen, and that the fast rate is an initial rate prior to the complete reduction of the enzyme. This problem should be more evident in the case of substrates with high turn-over rate and to some extent this is what we observe. To test this hypothesis, we used 5NQ as a reducing substrate to substitute for oxygen in the enzyme cycle. Since 5NQ reduction is a 6-electron reduction we would observe a change in the enzyme activity if electron transfer has become rate-limiting once we substitute this substrate for molecular oxygen which only needs 2 electrons to be reduced. 5NQ is reduced by AOX to 5-aminoquinoline. Unlike its isomer, 6-nitroquinoline, 5NQ can be both oxidized and reduced by AOX under normal oxygen condition (Rajapakse et al., 2013). Time-course results indicate that we do see a change in activity with alternate reducing substrate as one would expect if electrons are transferred more slowly (Fig. 8). This is consistent with our previous results showing that once an oxidative substrate is present, 5NQ has an increased affinity for the flavin site where it can compete with oxygen (Paragas et al., 2017a). This can lead to a disruption in enzyme oxidation and may be the reason for the observed loss in enzyme activity. While this is consistent with the data, the complicated kinetics means that a number of possibilities are likely since a few factors can affect electron flow through the enzyme.

Discussion:

After monitoring the changes in AOX activity over time in both HAO and HLC for six oxidative substrates. We found that the enzyme does not behave linearly over time for most substrates. We used three different kinetic models to determine what was likely happening kinetically over time. Initially we assumed that the enzyme loses its activity completely over time, in other words it dies. This leads to better fits than the MM model, but still does not describe the data very well. The next hypothesis was that the enzyme is altered over time and therefore runs with a lower efficiency after a certain period of time, this gave the best fits for all of the substrates except zoniporide. Representative fits to each model, for the substrate O6BG, are shown in Fig. 4 and for all substrate in supplemental information.

Next, we checked for possible reasons behind loss of activity in AOX. Although it has been mentioned before that superoxide has little effect on biological molecules and enzymes, there have been instances like cytochrome c where it does compromise enzyme activity often by oxidation of thiols (Searle and Willson, 1980; Kundu et al., 2007). To check if ROS altered enzyme activity, we decided to also check the effect by removing them with SOD and catalase. Based on the results, no significant change in enzyme linearity was observed with or without using ROS scavengers showing that ROS are not altering enzymatic behavior.

Substantial decrease in substrate concentration can also lead to similar changes in enzyme linearity but this hypothesis was rejected by determining the amount of oxidative substrate depletion. Simulation results for the substrates show that most of the substrates are not extensively consumed from their initial concentration and since the initial concentrations was five times the K_m this

DMD Fast Forward. Published on February 20, 2019 as DOI: 10.1124/dmd.118.085787
This article has not been copyedited and formatted. The final version may differ from this version.

should not lead to nonlinear kinetics (Fig. 7). As for the reductive substrate of AOX, O_2, (Garattini et al., 2003; Pryde et al., 2010) we have determined that its K_m is approximately 2-16 μM and based on the atmospheric pressure where the experiment was done, the concentration of oxygen is around 213 μM. We know that among the substrates that we used, even the substrate with the fastest turn-over rate would only consume between 20-40 μmoles of oxygen leaving the concentration in the reaction vial more than 5 times the K_m and the reaction would be zero order with respect to oxygen

To regenerate AOX after oxidation of substrate we need to transfer electrons from the Moco through the iron-sulfur clusters to the FAD before we reduce oxygen. If this electron transfer path is slow, reduced AOX will build-up and reduction of oxygen will become the rate-limiting step. This is consistent with the fact that a kinetic isotope effect was observed upon substrate oxidation on V/K but not V_{max} (Alfaro et al., 2009). This hypothesis is also consistent with our time-course plots where the fast initial rate decreases as more and more enzymes get trapped in their reduced state. To test this hypothesis we used 5NQ as a source of reductive substrate that will compete with oxygen in accepting electrons from AOX to check whether a disruption of electron transfer is the reason behind the loss in enzyme activity. Since 5NQ needs 6 electrons to get reduced to 5-aminoquinoline (Paragas et al., 2017a), this should change the rate of the second kinetic phase after the enzyme becomes reduced. The data in Fig. 8 is consistent with the slowing of electron transfer and a change in the rate-limiting step from oxidation to reduction. However, one caveat with this conclusion is that the rates for the slow reaction (k_5) for all the substrates should be the same, since the rate limiting step on the second kinetic phase of the reaction is the oxidation of enzyme by O_2 and should be substrate independent. However, looking at the k_5 values for the

substrates we can see up to a 3-fold difference. In addition to that, if this was the case, we would also expect similar looking plots for substrates that exhibit similar k_3 values such as DACA and O6BG. But looking at the plots, we can see O6BG time-course plot looks much more linear than DACA. This can be explained if we consider the effect of substrate inhibition. It appears that O6BG does not show any substrate inhibition (Barr et al., 2015) while the reported K_I value for DACA was 91 μM (Paragas et al., 2017b). We hypothesize that the second substrate molecule would bind to the reduction site and therefore make the reduction happen even more slowly, the same effect that we saw by using a reductive substrate 5NQ, and that is why the k_5 value for DACA is lower than that of O6BG. It is also worth mentioning that phthalazine also exhibits substrate inhibition and the reported value of K_I for this substrate is 250 μM (Obach et al., 2004). However since DACA is a more effective inhibitor of electron transfer to oxygen compared with pthalazine, DACA has a slower rate in the second kinetic phase. Attempts to fit substrate inhibition did not improve the overall fit, as might be expected, given that the model already can fit each single substrate dataset very well. The fits are given in supplemental Figure 2 for O-6BG.

In this work, the intrinsic clearance values were also compared using the rate constants derived from the MAM and MM models. The results show a significant improvement of clearance estimation for MAM. Given that the initial rate calculations only account for how the enzyme behaves for a very short period of time, longer incubation times are needed for a more comprehensive assessment of the enzyme kinetics. Using the MM model leads to a considerable underprediction of intrinsic clearance in vitro due to negligence towards the fast initial turn-over rate. One assumption behind the residual underprediction using MAM can be referred back to the involvement of extrahepatic clearance. This factor has also been considered for in silico estimation

of intrinsic clearance by AO (Jones and Korzekwa, 2013) and the in vivo-in vitro correlation plot is consistant with this assumption (Supplemental Fig. 5).We admit that we cannot be certain this is the case, although the known underestimation of V/K supports this conclusion. Futhermore the rate of reaction, to some extent, can be predicted by the reactivity of the substrate that is oxidized, while if the second phase is oxidation of the enzyme no such correlation would be expected to exist (Zhang et al., 2018)

Overall, the main goal of this paper is to show that almost all AOX catalyzed reactions are nonlinear over time, and that ignoring this leads to an underestimation of clearance. We have shown that there can be up to 40-fold under-prediction of the reaction rate by simply assuming linear kinetics. We believe that the constant under-prediction of drug clearance by AOX is due to the rapid slowing of the reaction rate once the reaction is started and that even short incubations would not lead to an accurate determination of the k_{cat}. In this paper, we are using numerical fitting to get the closest approximation of the real initial rate value by fitting the metabolite formation over 4-hour period instead of only using the short "linear" region of the plot. MAM seems to do well in describing the enzymatic pathway in which the enzyme's life is divided into two stages. The first one being a fully active enzyme and the second being the stage where the enzyme forms metabolite at a slower rate.

Acknowledgements

We would like to thank Dr. Dmitri R. Davydov for helping with oxygen K_m measurements.

Authorship Contributions

Participation in research design: Abbasi, Rodgers, and Jones.

Performed data analysis: Abbasi, Paragas, and Joswig-Jones.

Wrote or contributed to the writing of the manuscript: Abbasi, Paragas, and Jones.

References:

Alfaro J, Joswig-Jones C, Ouyang W, Nichols J, Crouch G, and Jones J (2009) Purification and mechanism of human aldehyde oxidase expressed in Escherichia coli. *Drug Metab Dispos* **37:**2393-2398.

Amano T, Fukami T, Ogiso T, Hirose D, Jones J, Taniguchi T, and Nakajima M (2018) Identification of enzymes responsible for dantrolene metabolism in the human liver: A clue to uncover the cause of liver injury. *Biochem Pharmacol* **151:**69-78.

Barr J, Choughule K, and Jones J (2014) Enzyme kinetics, inhibition, and regioselectivity of aldehyde oxidase, in: *Enzyme kinetics in drug metabolism: fundamentals and applications* (Nagar S, Argikar U, and Tweedie D eds), pp 167-186.

Barr J and Jones J (2013) Evidence for substrate-dependent inhibition profiles for human liver aldehyde oxidase. *Drug Metab Dispos* **41:**24-29.

Barr J, Jones J, Joswig-Jones C, and Rock D (2013) Absolute quantification of aldehyde oxidase protein in human liver using liquid chromatography-tandem mass spectrometry. *Mol Pharm* **10:**3842-3849.

Barr J, Jones J, Oberlies N, and Paine M (2015) Inhibition of human aldehyde oxidase activity by diet-derived constituents: structural influence, enzyme-ligand interactions, and clinical relevance. *Drug Metab Dispos* **43:**34-41.

Crouch RD, Hutzler JM, and Daniels JS (2018) A novel in vitro allometric scaling methodology for aldehyde oxidase substrates to enable selection of appropriate species for traditional allometry. *Xenobiotica* **48:**219-231.

Dalvie D, Kang P, Loi CM, Goulet L, and Nair S (2010a) *Influence of Heteroaromatic Rings on ADME Properties of Drugs*.

Dalvie D, Zhang C, Chen W, Smolarek T, Obach RS, and Loi C-M (2010b) Cross-Species Comparison of the Metabolism and Excretion of Zoniporide: Contribution of Aldehyde Oxidase to Interspecies Differences. *Drug Metab Dispos* **38:**641-654.

Garattini E, Fratelli M, and Terao M (2008) Mammalian aldehyde oxidases: genetics, evolution and biochemistry. *Cell Mol Life Sci* **65:**1019-1048.

Garattini E, Mendel R, Romao MJ, Wright R, and Terao M (2003) Mammalian molybdo-flavoenzymes, an expanding family of proteins: structure, genetics, regulation, function and pathophysiology. *Biochem J* **372:**15-32.

Garattini E and Terao M (2012) The role of aldehyde oxidase in drug metabolism. *Expert Opin Drug Metab Toxicol* **8:**487-503.

Hutzler J and Tracy T (2002) Atypical kinetic profiles in drug metabolism reactions. *Drug Metab Dispos* **30:**355-362.

Hutzler M, Yang Y, Albaugh D, Fullenwider C, Schmenk J, and Fisher M (2012) Characterization of aldehyde oxidase enzyme activity in cryopreserved human hepatocytes. *Drug Metab Dispos* **40:**267-275.

Jones JP and Korzekwa KR (2013) Predicting Intrinsic Clearance for Drugs and Drug Candidates Metabolized by Aldehyde Oxidase. *Mol Pharm* **10:**1262-1268.

Kaye B, Offerman JL, Reid JL, Elliott HL, and Hillis WS (1984) A species-difference in the presystematic metabolism of carbazeran in dog and man. *Xenobiotica* **14:**935-945.

Kitamura S and Tatsumi K (1984) Involvement of liver aldehyde oxidase in the reduction of nicotinamide N-oxide. *Biochem Biophys Res Commun* **120:**602-606.

Konishi K, Fukami T, Gotoh S, and Nakajima M (2017) Identification of enzymes responsible for nitrazepam metabolism and toxicity in human. *Biochem Pharmacol* **140:**150-160.

Korzekwa KR, Krishnamachary N, Shou M, Ogai A, Parise RA, Rettie AE, Gonzalez FJ, and Tracy TS (1998) Evaluation of atypical cytochrome P450 kinetics with two-substrate models: evidence that multiple substrates can simultaneously bind to cytochrome P450 active sites. *Biochemistry* **37:**4137-4147.

Krenitsky TA, Neil SM, Elion GB, and Hitchings GH (1972) A COMPARISON OF THE SPECIFICITIES OF XANTHINE OXIDASE EC-1.2.3.2 AND ALDEHYDE OXIDASE EC-1.2.3.1. *Arch Biochem Biophys* **150:**585-599.

Kundu T, Hille R, Velayutham M, and Zweier J (2007) Characterization of superoxide production from aldehyde oxidase: an important source of oxidants in biological tissues. *Arch Biochem Biophys* **460:**113-121.

Li H, Kundu T, and Zweier J (2009a) Characterization of the magnitude and mechanism of aldehyde oxidase-mediated nitric oxide production from nitrite. *J Biol Chem* **284:**33850-33858.

Li HT, Kundu TK, and Zweier JL (2009b) Aldehyde oxidase catalyzes nitrite reduction: an important nitric oxide producing pathway during ischemia. *Faseb J* **23**.

Lynch T and Price A (2007) The effect of cytochrome P450 metabolism on drug response, interactions, and adverse effects. *Am Fam Physician* **76:**391-396.

Maia L, Pereira V, Mira L, and Moura J (2015) Nitrite reductase activity of rat and human xanthine oxidase, xanthine dehydrogenase, and aldehyde oxidase: evaluation of their contribution to NO formation in vivo. *Biochemistry* **54:**685-710.

Mendel RR (2009) Cell biology of molybdenum. *Biofactors* **35:**429-434.

Obach RS, Huynh P, Allen MC, and Beedham C (2004) Human liver aldehyde oxidase: Inhibition by 239 drugs. *J Clin Pharmacol* **44:**7-19.

Paragas EM, Humphreys SC, Min J, Joswig-Jones CA, and Jones JP (2017a) The two faces of aldehyde oxidase: Oxidative and reductive transformations of 5-nitroquinoline. *Biochem Pharmacol* **145:**210-217.

Paragas EM, Humphreys SC, Min J, Joswig-Jones CA, Leimkuhler S, and Jones JP (2017b) ecoAO: A Simple System for the Study of Human Aldehyde Oxidases Role in Drug Metabolism. *ACS Omega* **2:**4820-4827.

Pryde DC, Dalvie D, Hu Q, Jones P, Obach RS, and Tran T-D (2010) Aldehyde oxidase: an enzyme of emerging importance in drug discovery. *J Med Chem* **53:**8441-8460.

Rajapakse A, Linder C, Morrison R, Sarkar U, Leigh N, Barnes C, Daniels S, and Gates K (2013) Enzymatic conversion of 6-nitroquinoline to the fluorophore 6-aminoquinoline selectively under hypoxic conditions. *Chem Res Toxicol* **26:**555-563.

Searle AJ and Willson RL (1980) Glutathione Peroxidase: Effect of Superoxide, Hydroxyl and Bromine Free Radicals on Enzyme Activity. *International Journal of Radiation Biology and Related Studies in Physics, Chemistry and Medicine* **37:**213-217.

Stoddart AM and Levine WG (1992) AZOREDUCTASE ACTIVITY BY PURIFIED RABBIT LIVER ALDEHYDE OXIDASE. *Biochem Pharmacol* **43:**2227-2235.

Weidert E, Schoenborn S, Cantu-Medellin N, Choughule K, Jones J, and Kelley E (2014) Inhibition of xanthine oxidase by the aldehyde oxidase inhibitor raloxifene: implications for identifying molybdopterin nitrite reductases. *Nitric Oxide* **37:**41-45.

Weiss RF (1970) The solubility of nitrogen, oxygen and argon in water and seawater. *Deep Sea Research* **17:**721-735.

Zhang JW, Xiao W, Gao ZT, Yu ZT, and Zhang JY (2018) Metabolism of c-Met kinase inhibitors containing quinoline by aldehyde oxidase, electron donating and steric hindrance effect. *Drug Metabolism and Disposition***:**dmd.118.081919.

Zientek M, Jiang Y, Youdim K, and Obach RS (2010) In Vitro-In Vivo Correlation for Intrinsic Clearance for Drugs Metabolized by Human Aldehyde Oxidase. *Drug Metab Dispos* **38:**1322-1327.

Footnotes

This work was supported by the National Institute of General Medical Sciences [GM100874].

Legends for Figures

Fig. 1. Summary of AOX-catalyzed reactions for the substrates used in this study.

Fig. 2. Five times the K_m amount of the substrates: A) O6BG, B) DACA, C) zaleplon, D) phthalazine E) BIBX1382, F) zoniporide were incubated with human liver cytosol (HLC, 0.0051 μM AO) at 37°C and samples were quenched at different time points over 240 minutes (n= 3, P< 0.001). Data fitting was performed using the MAM. Based on the results unlike the MM assumption, the enzyme activity is not linear over time.

Fig. 3. Five times the K_m amount of the substrates: A) O6BG, B) DACA, C) zaleplon, D) phthalazine E) BIBX1382, F) zoniporide were incubated with Purified expressed human AOX (HAO, 0.0192 μM) in the same way as HLC to compare the time-course plots and make sure AOX is the enzyme responsible for metabolism. Fitting to product formation was performed using the MAM (n= 3, P< 0.001).

Fig. 4. Two different kinetic models were developed to compare the numerical fitting of time-course data with MM. A) MM model, B) Dead enzyme model, C) MAM. Akaike values were provided by Mathematica to compare the goodness of fit proving the MAM is the best model to fit the time-course data for most substrates except for zoniporide. Data fitting plots for O6BG is provided next to each kinetic scheme for comparison. The Akaike values for O6BG are provided on the bottom right side of each plot.

DMD Fast Forward. Published on February 20, 2019 as DOI: 10.1124/dmd.118.085787
This article has not been copyedited and formatted. The final version may differ from this version.

Fig. 5. Catalase and super oxide dismutase (SOD, 250 U/ml) were used to remove reactive oxygen species (ROS) that were suspected to affect the enzymatic activity. Human liver cytosol (HLC, 0.0051 μM AO) was used to start the reactions (n= 3, P< 0.001). No significant change in linearity of the enzyme was observed once these reagents were used suggesting that ROS are not the reason behind the decrease in enzymatic efficacy.

Fig. 6. Catalase and super oxide dismutase (SOD, 250 U/ml) were used to remove reactive oxygen species (ROS) that were suspected to affect the enzymatic activity for purified HAO. No significant change in linearity of the enzyme was observed once these reagents were used suggesting that ROS are not the reason behind the decrease in enzymatic efficacy.

Fig. 7. Substrate consumption simulation for A) O6BG, B) DACA, C) zaleplon and D) phthalazine were done using the kinetic parameters obtained from fitting the product formation data in purified expressed human AOX (HAO) to the MAM using Mathematica. This could not be done for the substrates which we do not have the product standards.

Fig. 8. Five times the K_m amount of the substrates were used with saturating amount of 5-nitroquinoline (5NQ, 200 μM) and HAO (0.0192 μM) was used to start the reaction (n= 3, P< 0.001).

DMD Fast Forward. Published on February 20, 2019 as DOI: 10.1124/dmd.118.085787
This article has not been copyedited and formatted. The final version may differ from this version.

Tables

TABLE 1

Rate constants related to each model for different substrates in HLC

substrate	rate constants	MAM	Dead model	MM
O6BG	k3 (1/min)	25.444	12.954	8.691
	k4 (1/min)	0.057	0.006	---
	k5 (1/min)	13.708	---	---
DACA	k3 (1/min)	33.004	19.449	6.209
	k4 (1/min)	0.044	0.024	---
	k5 (1/min)	6.086	---	---
zaleplon	k3 (1/min)	1.238	0.853	0.46
	k4 (1/min)	0.028	0.011	---
	k5 (1/min)	0.604	---	---
phthalazine	k3 (1/min)	466.834	351.727	11.086
	k4 (1/min)	0.335	0.366	---
	k5 (1/min)	8.523	---	---
BIBX*	k3 (1/min)	0.279	0.253	0.125
	k4 (1/min)	0.012	0.012	---
	k5 (1/min)	0.097	---	---
zoniporide*	k3 (1/min)	0.082	0.079	0.085
	k4 (1/min)	-0.023	-0.001	---
	k5 (1/min)	0.163	---	---

*rate constants are based on peak area ratio (PAR)

DMD Fast Forward. Published on February 20, 2019 as DOI: 10.1124/dmd.118.085787
This article has not been copyedited and formatted. The final version may differ from this version.

TABLE 2

Rate constants related to each model for different substrates in HAO.

substrate	rate constants	MAM	Dead model	MM
O6BG	k3 (1/min)	21.955	16.154	6.896
	k4 (1/min)	0.025	0.016	---
	k5 (1/min)	7.003	---	---
DACA	k3 (1/min)	23.282	20.353	6.307
	k4 (1/min)	0.020	0.025	---
	k5 (1/min)	3.577	---	---
zaleplon	k3 (1/min)	6.248	3.387	1.660
	k4 (1/min)	0.044	0.013	---
	k5 (1/min)	2.152	---	---
phthalazine	k3 (1/min)	167.355	79.953	4.403
	k4 (1/min)	0.489	0.246	---
	k5 (1/min)	5.195	---	---
BIBX1382*	k3 (1/min)	5.971	2.673	1.679
	k4 (1/min)	0.070	0.012	---
	k5 (1/min)	2.157	---	---
zoniporide*	k3 (1/min)	0.412	0.412	0.400
	k4 (1/min)	-0.0002	0.0005	---
	k5 (1/min)	1.825	---	---

*rate constants are based on PAR

DMD Fast Forward. Published on February 20, 2019 as DOI: 10.1124/dmd.118.085787
This article has not been copyedited and formatted. The final version may differ from this version.

TABLE 3

Comparison between intrinsic clearance in HAO between different models in vitro and the in vivo intrinsic clearance in literature.

Drug	**$Cl'_{int,AO}$ (in vitro, ml/(min.kg))**			**$Cl'_{int,AO}$ (in vivo, ml/(min. kg))**	**Reference**
	MAM (using k3)	**MAM (using k5)**	**MM**		
O6BG	202	65	64	360	(Dolan et al., 1998)
DACA	1183	182	320	3600	(Kestell et al., 1999)
zaleplon	43	15	11	65	(Rosen et al., 1999)

DMD Fast Forward. Published on February 20, 2019 as DOI: 10.1124/dmd.118.085787
This article has not been copyedited and formatted. The final version may differ from this version.

Figures

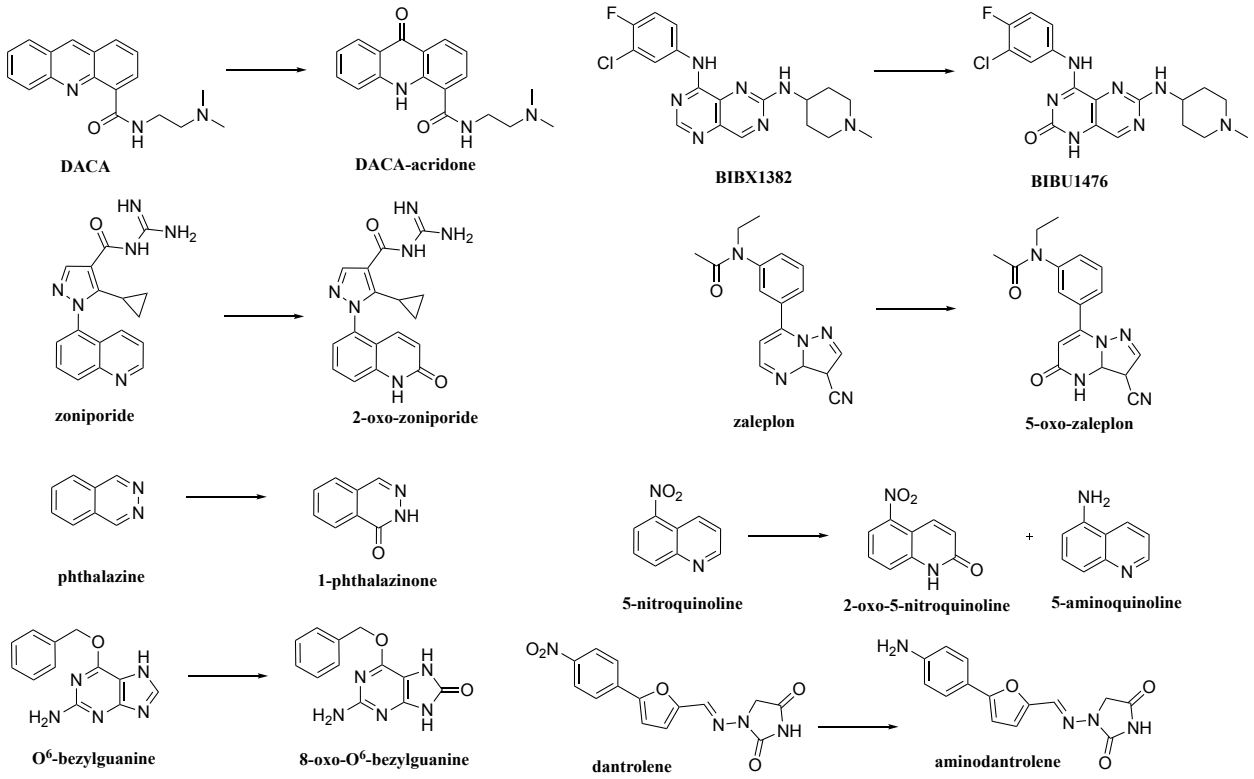

Fig. 1.

DMD Fast Forward. Published on February 20, 2019 as DOI: 10.1124/dmd.118.085787
This article has not been copyedited and formatted. The final version may differ from this version.

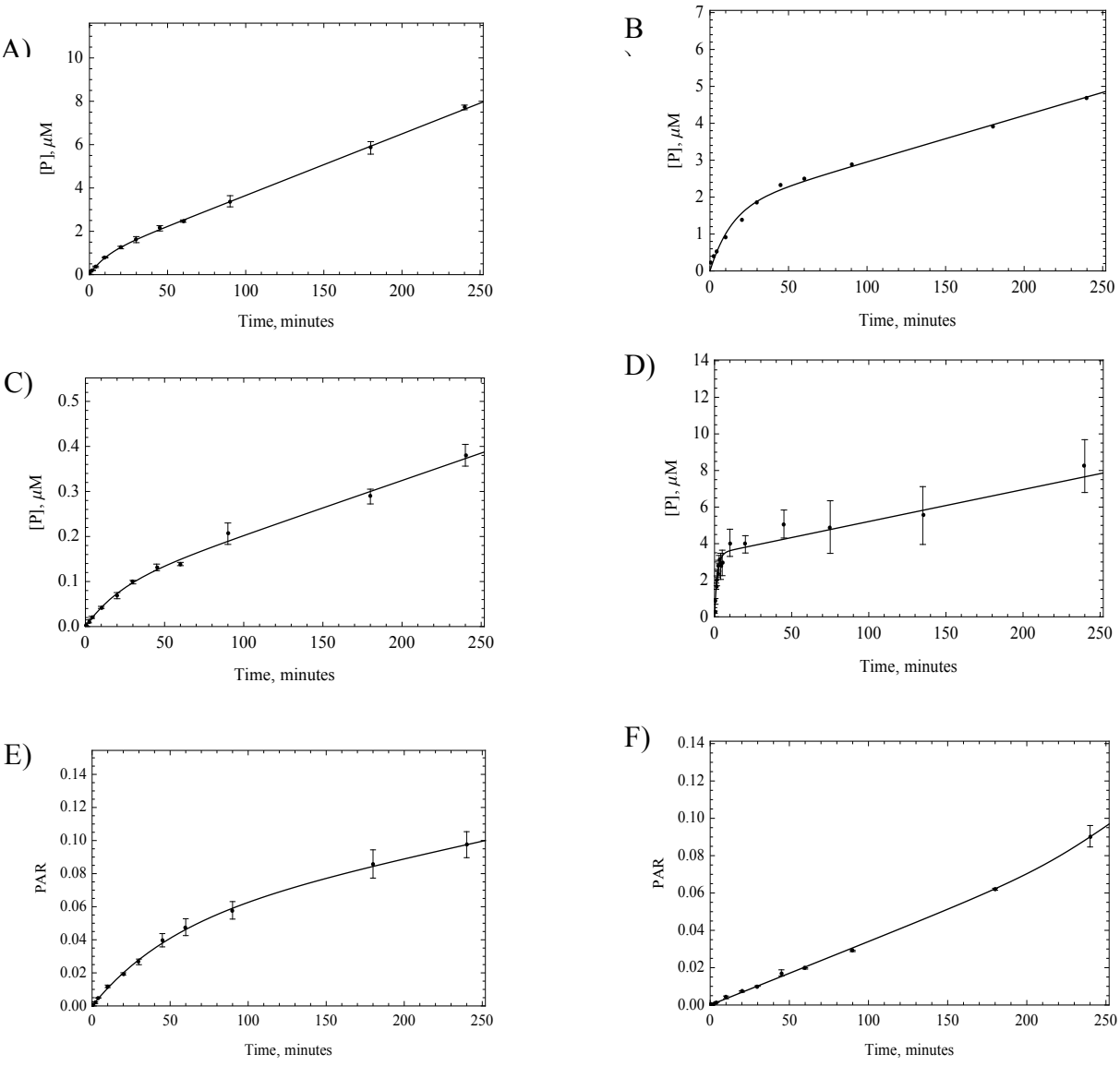

Fig. 2.

DMD Fast Forward. Published on February 20, 2019 as DOI: 10.1124/dmd.118.085787
This article has not been copyedited and formatted. The final version may differ from this version.

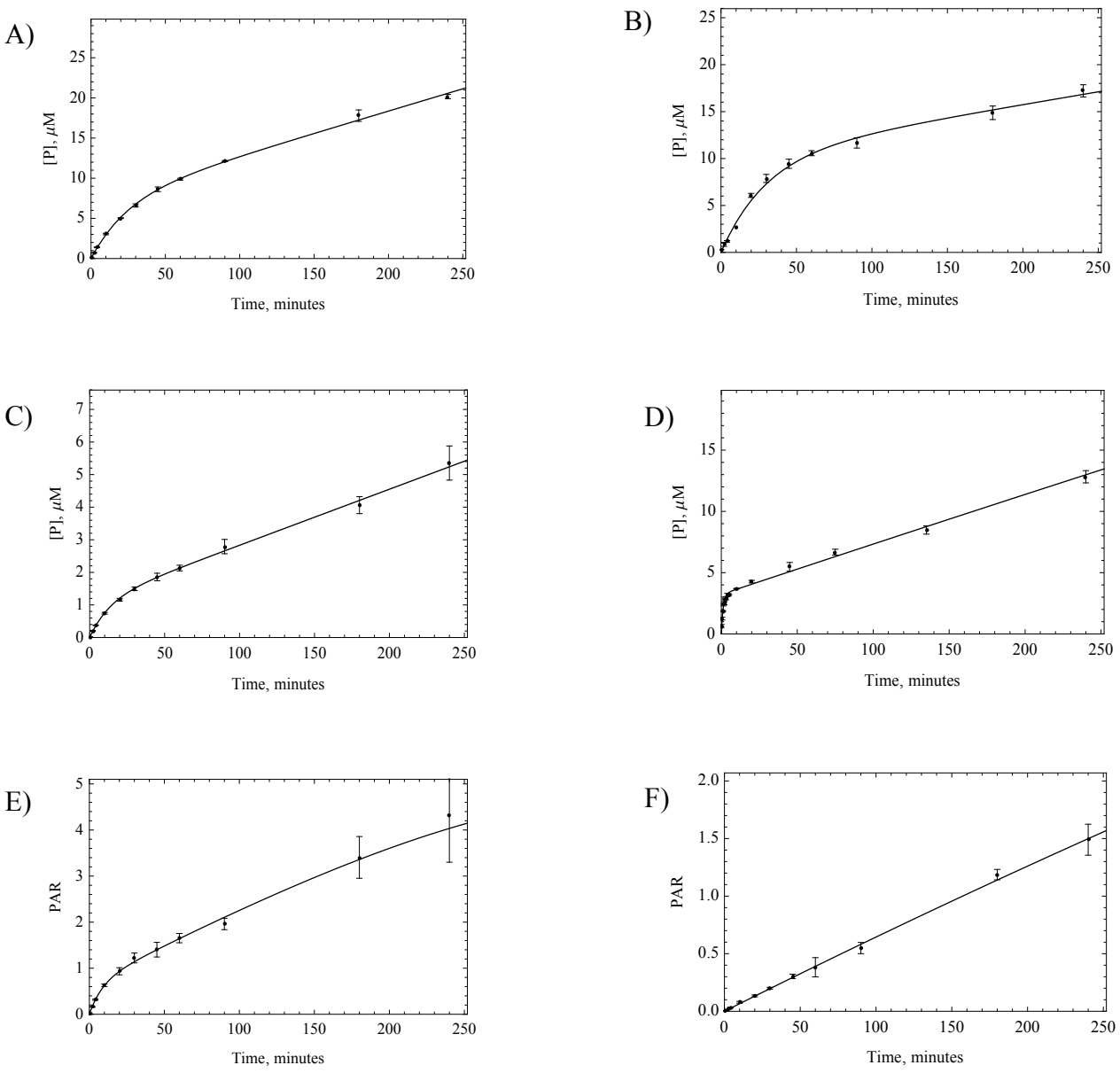

Fig. 3.

DMD Fast Forward. Published on February 20, 2019 as DOI: 10.1124/dmd.118.085787
This article has not been copyedited and formatted. The final version may differ from this version.

A)

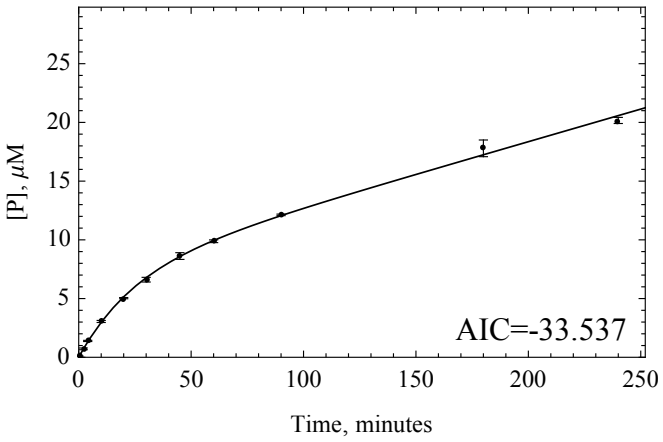

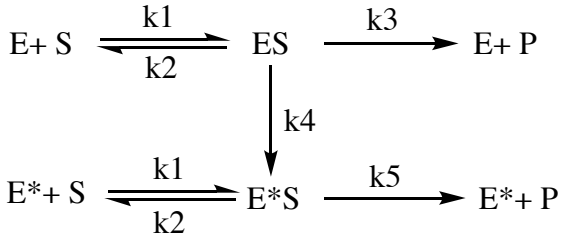

B)

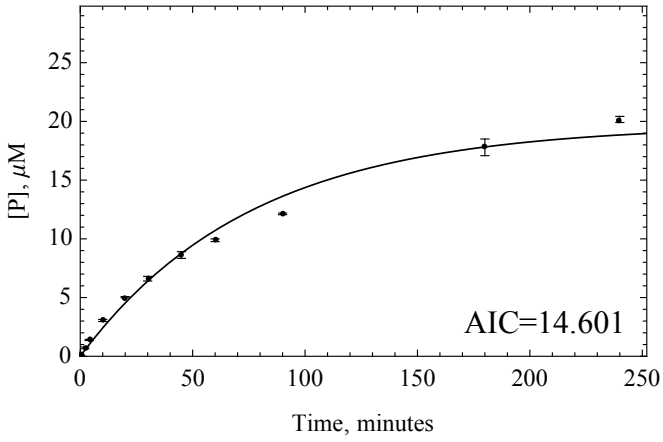

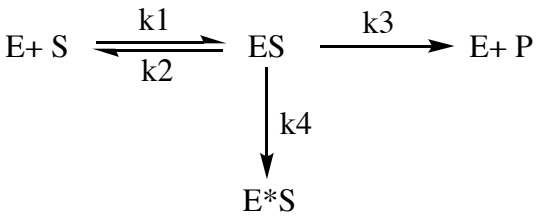

C)

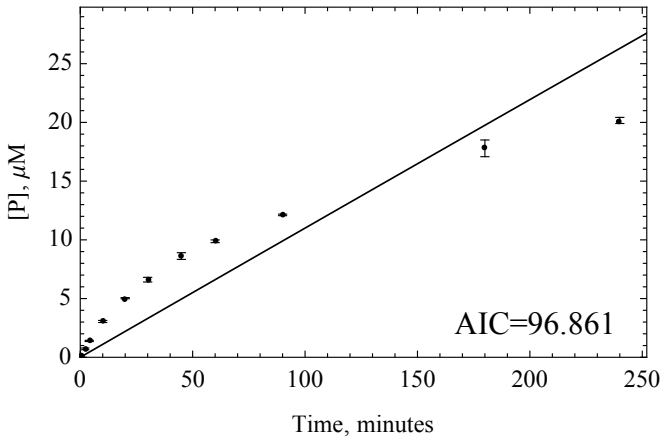

Fig. 4.

DMD Fast Forward. Published on February 20, 2019 as DOI: 10.1124/dmd.118.085787
This article has not been copyedited and formatted. The final version may differ from this version.

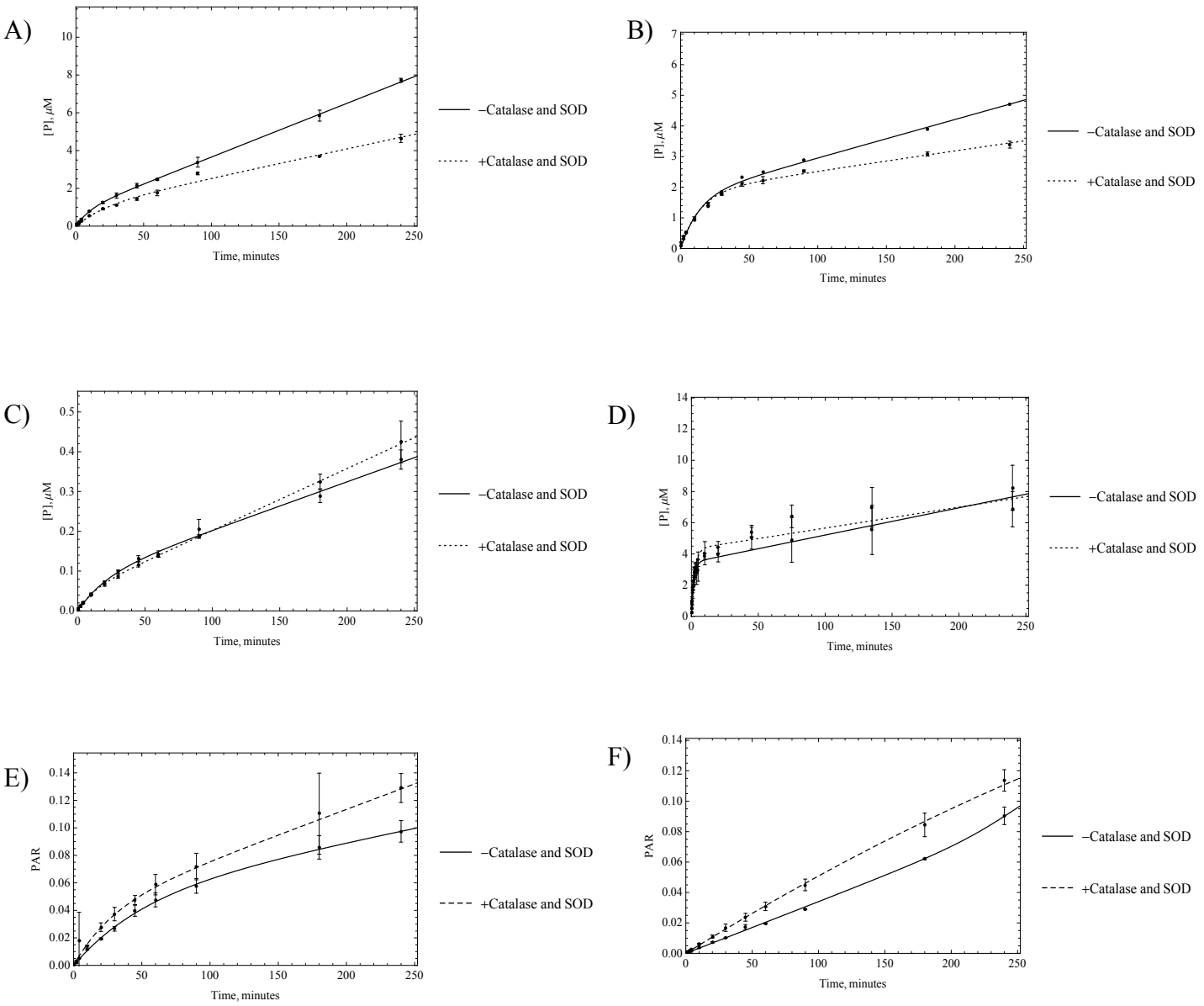

Fig. 5.

DMD Fast Forward. Published on February 20, 2019 as DOI: 10.1124/dmd.118.085787
This article has not been copyedited and formatted. The final version may differ from this version.

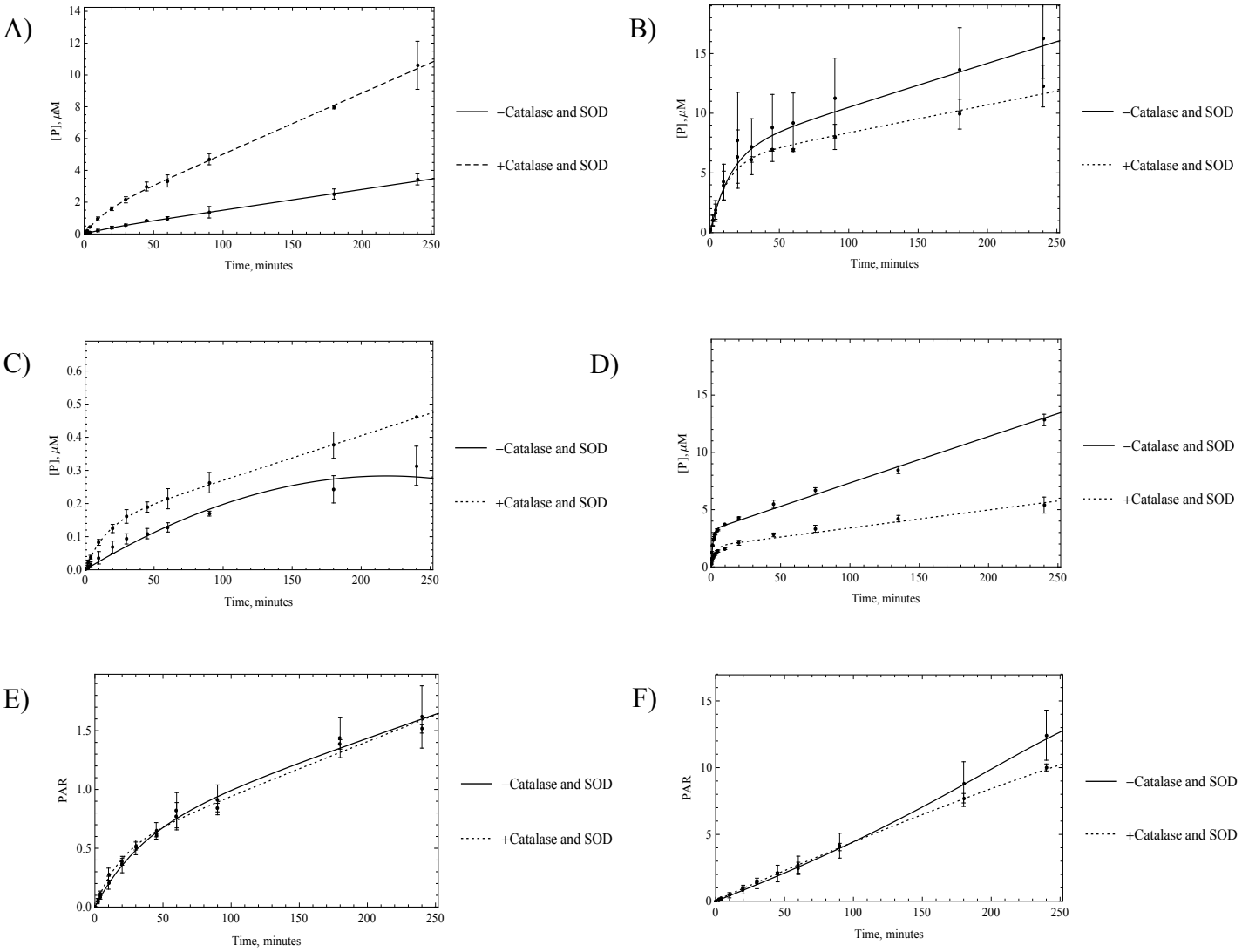

Fig. 6.

DMD Fast Forward. Published on February 20, 2019 as DOI: 10.1124/dmd.118.085787
This article has not been copyedited and formatted. The final version may differ from this version.

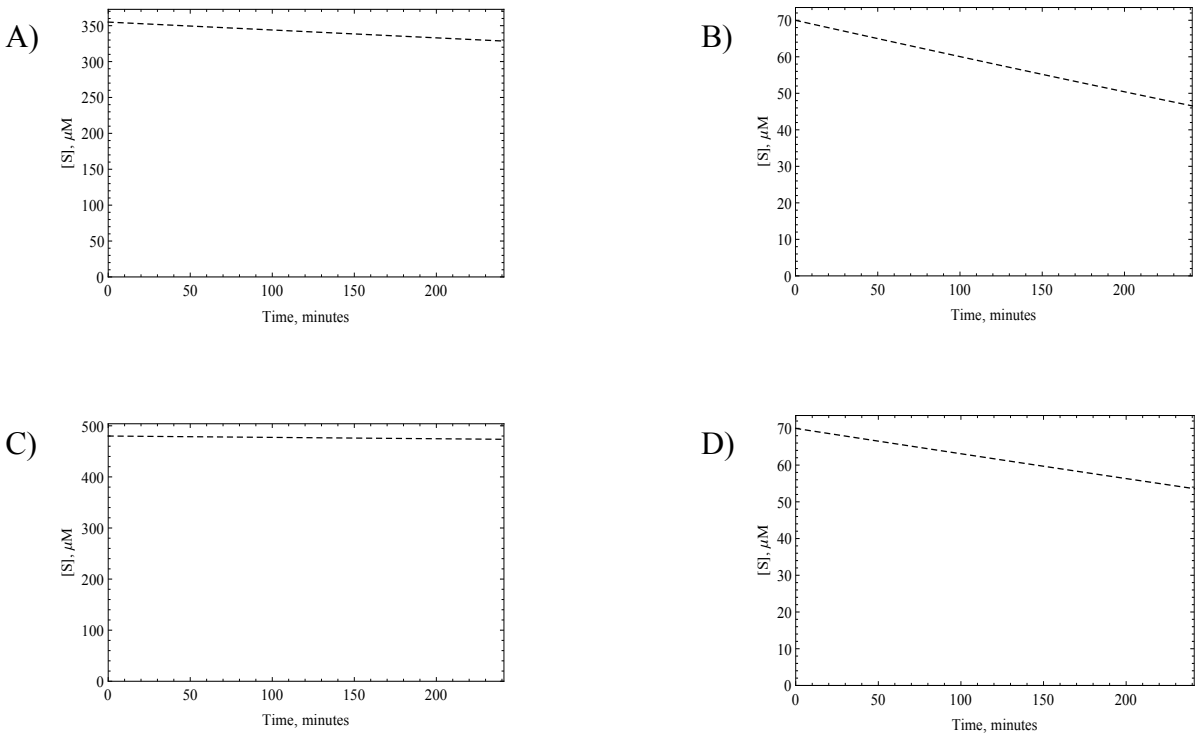

Fig. 7.

DMD Fast Forward. Published on February 20, 2019 as DOI: 10.1124/dmd.118.085787
This article has not been copyedited and formatted. The final version may differ from this version.

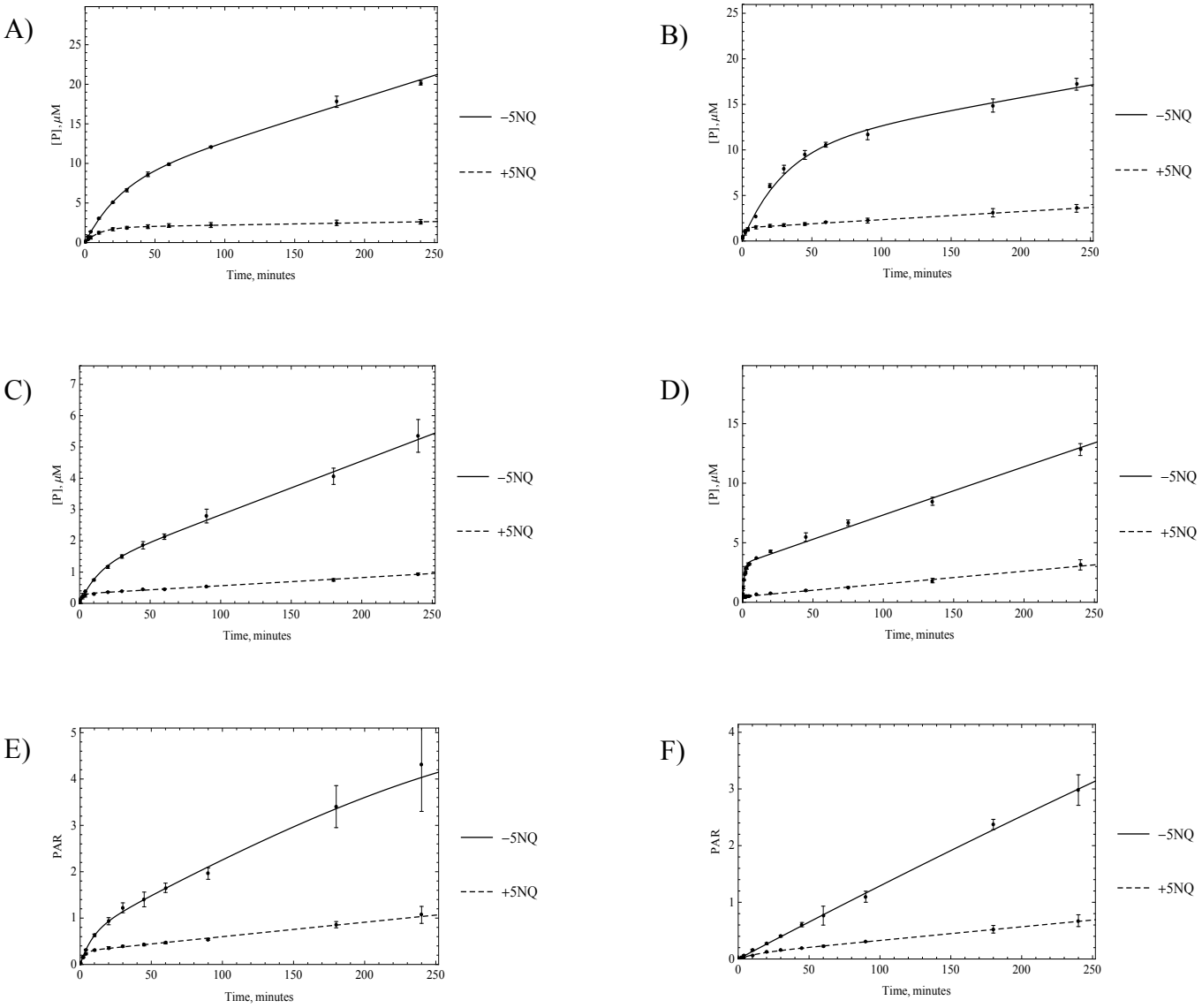

Fig. 8.